Journal of Crystal Growth 321 (2011) 176–182

Contents lists available at ScienceDirect

Journal of Crystal Growth

journal homepage: www.elsevier.com/locate/jcrysgro

A fast, robust, and accurate operator splitting method for phase-field simulations of crystal growth

Yibao Li, Hyun Geun Lee, Junseok Kim *

Department of Mathematics, Korea University, Seoul 136-701, Republic of Korea

ARTICLE INFO

Article history:
Received 30 August 2010
Received in revised form
27 October 2010
Accepted 25 February 2011
Communicated by J.J. Derby
Available online 4 March 2011

Keywords:
A2. Crystal growth
A1. Phase-field simulation
A1. Operator splitting
A1. Multigrid method

ABSTRACT

In this paper we propose a fast, robust, and accurate operator splitting method for phase-field simulations of dendritic growth in both two- and three-dimensional space. The proposed method is based on operator splitting techniques. We split the governing phase-field equation into three parts: the first equation is calculated by using an explicit Euler's method. The second is a heat equation with a source term and is solved by a fast solver such as a multigrid method. The third is a nonlinear equation and is evaluated using a closed form solution. We also present a set of representative numerical experiments for crystal growth simulation to demonstrate the accuracy and efficiency of the proposed method. Our simulation results are also consistent with previous numerical experiments.

© 2011 Elsevier B.V. All rights reserved.

1. Introduction

Crystal growth is a classical example of phase transformations from the liquid phase to the solid phase via heat transfer. For several decades, to understand and simulate crystal growth, several methods have been developed including boundary integral [1–4], cellular automaton [5–8], front-tracking [9–13], level-set [14–17], Monte-Carlo [18,19], and phase-field [20–37] methods. Among these various methods, the phase-field method is popular and widely used. Its advantage is that the explicit tracking of the interface is unnecessary by introducing an order parameter, i.e., a phase-field variable. In this paper, we focus on the phase-field method for crystal growth problems which avoids difficulties associated with tracking the interface and computes complex crystal shapes.

We consider here the solidification of a pure substance from its supercooled melt in both two- and three-dimensional space. A great challenge in the simulation with various supercoolings is the large difference in time and length scales. In order to overcome this, many numerical methods have been proposed such as explicit [11,27,31,36,38], mixed implicit-explicit [30,35,37], and adaptive [21,22,29,32,33] methods. In explicit methods, which are widely used, the solutions become unstable for large time steps. For this reason the authors in [11,36] suggested $\Delta t < h^2/(4D)$ for stability of explicit methods. Here, Δt is the time step, h is the mesh size, and D is the thermal diffusivity. In [11], the time step is also restricted to $\Delta t \le h/(10|V_{\max}|)$, where $|V_{\max}|$ is the magnitude of the maximum value of the interface velocity. Also the authors in [36] showed that $\Delta t = h^2/(5D_L)$ works well for not too large choices of the anisotropy by numerical experiments, where $D_L = M_\phi \varepsilon^2$, M_ϕ is the kinetic mobility, and ε is the interface energy anisotropy. Implicit methods allow relatively larger time steps, however, they are computationally more expensive per step than explicit ones. Another classical method is a multiple time-step algorithm that uses a larger time step for the flow-field calculations while reserving a finer time step for the phase-field evolution [34]. The use of mesh adaptivity is a natural choice to overcome this problem. However, explicit adaptive technology also suffers the time step restriction. Therefore, we need a scheme that allows the use of a sufficiently large time step without the technical limitations. In this paper we present a new, computationally efficient, and robust operator splitting algorithm for solving phase-field simulations of dendritic growth and demonstrate the accuracy and efficiency of the method by a set of representative numerical experiments.

This paper is organized as follows: in Section 2 the governing equations for crystal growth based on the phase-field method are given. In Section 3 we describe the computationally efficient operator splitting algorithm. In Section 4 we present numerical results for solving the crystal growth simulation both in 2D and 3D. Finally, conclusions are given in Section 5.

2. The phase-field model

The basic equations of the phase-field model are derived from a single Lyapounov functional [39]. We model the solidification in

* Corresponding author. Tel.: +82 2 3290 3077; fax: +82 2 929 8562.
E-mail address: cfdkim@korea.ac.kr (J. Kim).
URL: http://math.korea.ac.kr/~cfdkim/ (J. Kim).

0022-0248/$ - see front matter © 2011 Elsevier B.V. All rights reserved.
doi:10.1016/j.jcrysgro.2011.02.042

two and three dimensions using a standard form of phase-field equations. The model is given by

$$\varepsilon^2(\phi)\frac{\partial\phi}{\partial t} = \nabla\cdot(\varepsilon^2(\phi)\nabla\phi)+[\phi-\lambda U(1-\phi^2)](1-\phi^2) + \left(|\nabla\phi|^2\varepsilon(\phi)\frac{\partial\varepsilon(\phi)}{\partial\phi_x}\right)_x + \left(|\nabla\phi|^2\varepsilon(\phi)\frac{\partial\varepsilon(\phi)}{\partial\phi_y}\right)_y + \left(|\nabla\phi|^2\varepsilon(\phi)\frac{\partial\varepsilon(\phi)}{\partial\phi_z}\right)_z, \quad (1)$$

$$\frac{\partial U}{\partial t} = D\Delta U+\frac{1}{2}\frac{\partial\phi}{\partial t}, \quad (2)$$

where ϕ is the order parameter, $\varepsilon(\phi)$ is the anisotropic function, λ is the dimensionless coupling parameter, and $U=c_p(T-T_M)/L$ is the dimensionless temperature field. Here c_p is the specific heat at constant pressure, T_M is the melting temperature, L is the latent heat of fusion, $D=\alpha\tau_0/\varepsilon_0^2$, α is the thermal diffusivity, τ_0 is the characteristic time, and ε_0 is the characteristic length. The order parameter is defined by $\phi=1$ in the solid phase and $\phi=-1$ in the liquid phase. The interface is defined by $\phi=0$ and λ is given as $\lambda=D/a_2$ with $a_2=0.6267$ [26,27]. For the four-fold symmetry, $\varepsilon(\phi)$ is defined as

$$\varepsilon(\phi)=(1-3\varepsilon_4)\left(1+\frac{4\varepsilon_4}{1-3\varepsilon_4}\frac{\phi_x^4+\phi_y^4+\phi_z^4}{|\nabla\phi|^4}\right),$$

where ε_4 is a parameter for the anisotropy of interfacial energy.

3. Numerical solution

In this section, we propose a robust hybrid numerical method for crystal growth simulation. For simplicity of exposition we shall discretize Eqs. (1) and (2) in two-dimensional space, i.e., $\Omega=(a,b)\times(c,d)$. Let N_x and N_y be positive even integers, $h=(b-a)/N_x$ be the uniform mesh size, and $\Omega_h=\{(x_i,y_j): x_i=(i-0.5)h,\ y_j=(j-0.5)h,\ 1\le i\le N_x, 1\le j\le N_y\}$ be the set of cell-centers. Let ϕ_{ij}^n be approximations of $\phi(x_i,y_j,n\Delta t)$, where $\Delta t=T/N_t$ is the time step, T is the final time, and N_t is the total number of time steps. The discrete differentiation operator is $\nabla_d\phi_{ij}=(\phi_{i+1,j}-\phi_{i-1,j},\phi_{i,j+1}-\phi_{i,j-1})/(2h)$. We then define the discrete Laplacian by $\Delta_d\phi_{ij}=(\phi_{i+1,j}+\phi_{i-1,j}-4\phi_{ij}+\phi_{i,j+1}+\phi_{i,j-1})/h^2$. We discretize Eqs. (1) and (2):

$$\varepsilon^2(\phi^n)\frac{\phi^{n+1}-\phi^n}{\Delta t} = \varepsilon^2(\phi^n)\Delta_d\phi^{n+1,2}+2\varepsilon(\phi^n)\nabla_d\varepsilon(\phi^n)\cdot\nabla_d\phi^n -F'(\phi^{n+1})-4\lambda U^nF(\phi^{n+1,1}) + \left(|\nabla_d\phi|^2\varepsilon(\phi)\frac{\partial\varepsilon(\phi)}{\partial\phi_x}\right)_x^n + \left(|\nabla_d\phi|^2\varepsilon(\phi)\frac{\partial\varepsilon(\phi)}{\partial\phi_y}\right)_y^n, \quad (3)$$

$$\frac{U^{n+1}-U^n}{\Delta t} = D\Delta_dU^{n+1}+\frac{\phi^{n+1}-\phi^n}{2\Delta t}, \quad (4)$$

where $F(\phi)=0.25(\phi^2-1)^2$ and $F'(\phi)=\phi(\phi^2-1)$. Here $\phi^{n+1,k}$ for $k=1,2$ are defined in the operator splitting scheme. We propose the following operator splitting scheme:

$$\varepsilon^2(\phi^n)\frac{\phi^{n+1,1}-\phi^n}{\Delta t} = 2\varepsilon(\phi^n)\nabla_d\varepsilon(\phi^n)\cdot\nabla_d\phi^n+\left(|\nabla_d\phi|^2\varepsilon(\phi)\frac{\partial\varepsilon(\phi)}{\partial\phi_x}\right)_x^n + \left(|\nabla_d\phi|^2\varepsilon(\phi)\frac{\partial\varepsilon(\phi)}{\partial\phi_y}\right)_y^n, \quad (5)$$

$$\varepsilon^2(\phi^n)\frac{\phi^{n+1,2}-\phi^{n+1,1}}{\Delta t} = \varepsilon^2(\phi^n)\Delta_d\phi^{n+1,2}-4\lambda U^nF(\phi^{n+1,1}), \quad (6)$$

$$\varepsilon^2(\phi^n)\frac{\phi^{n+1}-\phi^{n+1,2}}{\Delta t} = -F'(\phi^{n+1}). \quad (7)$$

In Eq. (5), we can simplify the following terms

$$|\nabla_d\phi|^2\frac{\partial\varepsilon(\phi)}{\partial\phi_x} = \frac{16\varepsilon_4\phi_x(\phi_x^2\phi_y^2-\phi_y^4)}{|\nabla_d\phi|^4},$$

$$|\nabla_d\phi|^2\frac{\partial\varepsilon(\phi)}{\partial\phi_y} = \frac{16\varepsilon_4\phi_y(\phi_x^2\phi_y^2-\phi_x^4)}{|\nabla_d\phi|^4}.$$

Eq. (7) can be considered as an approximation of the equation

$$\phi_t=\frac{\phi-\phi^3}{\varepsilon^2} \quad (8)$$

by an implicit Euler's method with the initial condition $\phi^{n+1,2}$. We can solve Eq. (8) analytically by the method of separation of variables [40]. The solution is given as follows:

$$\phi^{n+1}=\frac{\phi^{n+1,2}}{\sqrt{e^{-2\Delta t/\varepsilon^2(\phi^n)}+(\phi^{n+1,2})^2\left(1-e^{-2\Delta t/\varepsilon^2(\phi^n)}\right)}}. \quad (9)$$

Finally, the proposed scheme can be written as follows:

$$\varepsilon(\phi^n)\frac{\phi^{n+1,1}-\phi^n}{\Delta t} = 2\varepsilon(\phi^n)_x\phi_x^n+2\varepsilon(\phi^n)_y\phi_y^n+\left(\frac{16\varepsilon_4\phi_x(\phi_x^2\phi_y^2-\phi_y^4)}{|\nabla_d\phi|^4}\right)_x^n + \left(\frac{16\varepsilon_4\phi_y(\phi_x^2\phi_y^2-\phi_x^4)}{|\nabla_d\phi|^4}\right)_y^n, \quad (10)$$

$$\varepsilon^2(\phi^n)\frac{\phi^{n+1,2}-\phi^{n+1,1}}{\Delta t} = \varepsilon^2(\phi^n)\Delta_d\phi^{n+1,2}-4\lambda U^nF(\phi^{n+1,1}), \quad (11)$$

$$\phi^{n+1}=\frac{\phi^{n+1,2}}{\sqrt{e^{-2\Delta t/\varepsilon^2(\phi^n)}+(\phi^{n+1,2})^2\left(1-e^{-2\Delta t/\varepsilon^2(\phi^n)}\right)}}, \quad (12)$$

$$\frac{U^{n+1}-U^n}{\Delta t} = D\Delta_dU^{n+1}+\frac{\phi^{n+1}-\phi^n}{2\Delta t}. \quad (13)$$

Eqs. (11) and (13) can be solved by a multigrid method [41,42].

3.1. Calculation of the crystal tip position and velocity

The crystal tip position and velocity are the important parameters in the phase-field simulation. To calculate these parameters with a high degree of accuracy we use a method based on the quadratic polynomial approximation. For simplicity, we only describe the procedure along the y-axis since the crystal is symmetric. Let y_k be the maximum y position on the interface at each time and the quadratic polynomial approximation be

$$y=\alpha x^2+\beta x+\gamma.$$

Given three points: (x_{k-1},y_{k-1}), (x_k,y_k), and (x_{k+1},y_{k+1}) on the interface, where one of the three y points is a maximum value along the interface points, we calculate the parameters α, β, and γ from

$$\begin{pmatrix}\alpha\\ \beta\\ \gamma\end{pmatrix}=\begin{pmatrix}x_{k-1}^2 & x_{k-1} & 1\\ x_k^2 & x_k & 1\\ x_{k+1}^2 & x_{k+1} & 1\end{pmatrix}^{-1}\begin{pmatrix}y_{k-1}\\ y_k\\ y_{k+1}\end{pmatrix}.$$

Then using α, β, and γ, we find the tip position (x_*,y_*) which satisfies the following conditions:

$$\left.\frac{dy}{dx}\right|_{x_*}=0 \quad \text{and} \quad y_*=\alpha x_*^2+\beta x_*+\gamma.$$

Furthermore, the crystal tip velocity can be obtained from the difference of tip positions at each time.

4. Numerical results

In this section we perform numerical experiments for two- and three-dimensional solidification to validate that our proposed scheme is accurate, efficient, and robust. For two-dimensional tests, unless otherwise specified, we take the initial state as

$$\phi(x,y,0)=\tanh\left(\frac{R_0-\sqrt{x^2+y^2}}{\sqrt{2}}\right) \quad \text{and} \quad U(x,y,0)=\begin{cases}0 & \text{if } \phi>0\\ \Delta & \text{else.}\end{cases}$$

The zero level set ($\phi=0$) represents a circle of radius R_0. From the dimensionless variable definition the value $U=0$ corresponds to the melting temperature of the pure material, while $U=\Delta$ is the initial undercooling. The extension to three dimensions is straightforward. The capillary length, d_0, is defined as $d_0=a_1/\lambda$ [20,32,39] with $a_1=0.8839$ [26,27,32] and $\lambda=3.1913$ [32]. And we take the value of the anisotropy of interfacial energy as $\varepsilon_4=0.05$.

4.1. Stability of the operator splitting algorithm

As already mentioned in Section 1, the previous methods suffer from time step restrictions $\Delta t\le O(h^2)$ for stability. In order to show the stability of our proposed method we consider the evolution of an interface with arbitrarily large time steps. In these simulations a 2048×2048 mesh is used on the computational domain $\Omega=(-200,200)^2$. We choose $R_0=14d_0$ and $\Delta=-0.55$. The calculations are run up to time $T=900$ with different time steps $\Delta t=0.3$ and $\Delta t=0.6$. Note that both time steps are larger than $h=400/2048\approx0.1953$. Figs. 1 (a) and (b) show evolutions of the interface with different time steps $\Delta t=0.3$ and 0.6, respectively. In general, large time steps may cause large truncation errors. However, as can be seen in Fig. 1 our proposed scheme works well with large time steps.

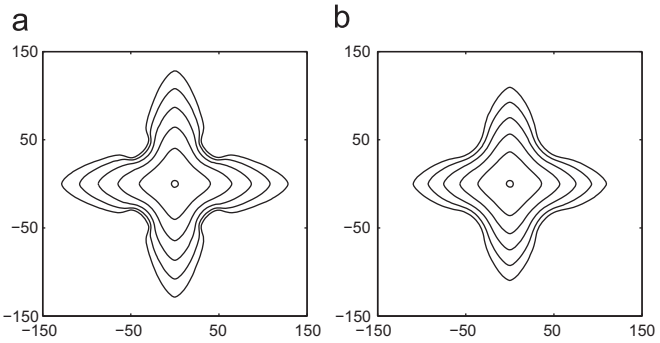

Fig. 1. (a) and (b) show the sequence of interfaces with different time steps $\Delta t=0.3$ and 0.6, respectively. The times are $t=0$, 180, 360, 540, 720, and 900 (from inside to outside).

Next, we perform a number of simulations on a set of increasingly finer grids to show that our proposed method is restricted by the stability constraint $\Delta t\le5.5$ h. The computational domain is $\Omega=(-200,200)^2$ and we take $R_0=14d_0$ and $\Delta=-0.55$. The numerical solutions are computed on the uniform grids $h=400/2^n$ with corresponding time steps $\Delta t=5.5h$ for $n=8$, 9, and 10. Fig. 2 shows the crystal growth after time $T=85.94$ with different time steps. From these results it is clear that our scheme is stable for time steps $\Delta t\le5.5h$. And we calculate the maximum Δt corresponding to different spatial grid sizes h so that stable solutions can be computed after 20 time step iterations. The results are shown in Table 1 and we obtain stable solutions for all three mesh sizes. Note that there is a linear relation between time step and mesh sizes. Thus, for finer mesh sizes we may use larger time steps than previous conventional methods.

4.2. Comparison of the dimensionless steady-state tip velocities

To verify the accuracy of our proposed scheme we compare the dimensionless steady-state tip velocities obtained by our proposed scheme with previous phase-field simulations and Green's function calculations [27]. A 1024×1024 mesh is used on the domain $\Omega=(-200,200)^2$. We choose $R_0=6.924$, $W_0=1$, and $\lambda=D/a_2$. Table 2 shows that the results from our proposed scheme are in good agreement with results of previous phase-field and Green's theory over the whole range of d_0,Δ, and ε_4 investigated here. Note that despite the relatively large time step ($\Delta t=5\Delta t^{KR}=0.08$) is used in our scheme, the results are almost identical.

4.3. Effect of time step, mesh, radius, and undercooling

We consider the evolution of the interface with different time steps in order to investigate the effect of time step. A 1024×1024 mesh is used on the domain $\Omega=(-400,400)^2$ with $R_0=14d_0$ and $\Delta=-0.55$. Figs. 3(a) and (b) show the position and velocity of the tip versus time, respectively, both for different time steps $\Delta t=0.6$, 0.3, 0.15, and 0.075. Fig. 3(c) shows the evolution of the interface with time step $\Delta t=0.15$ at times $t=0$, 225, 450, 675, 900, 1125, 1350, 1575, and 1800 (from inside to outside). For different time steps, the interfaces at time $T=1800$ are shown in Fig. 3(d). The velocity of the tip at time $T=1800$ versus time step is shown in Fig. 4. The results suggest that the convergence rate of the tip velocity is linear with respect to the time step.

Total CPU and average CPU ($\overline{\text{CPU}}$) times of the simulations for different time steps are listed in Table 3. The average CPU time is defined as the real computational time (excluding data printing times) divided by the total number of iterations.

Next we consider the evolution of the interface with different mesh sizes. 256×256, 512×512, 1024×1024, and 2048×2048 meshes are used on the domain $\Omega=(-200,200)^2$, i.e., we use four different $h=1.5626$, 0.7813, 0.3906, and 0.1953. The parameters used are $R_0=14d_0$, $\Delta=-0.55$, $\Delta t=0.15$, and $T=900$. Figs. 5(a)–(d)

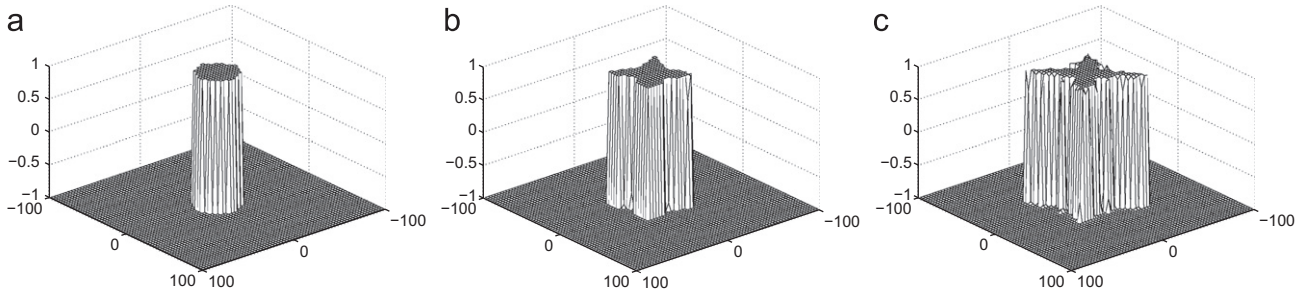

Fig. 2. The stability of crystal growth with different time steps: (a) $\Delta t=8.60$ (256×256 mesh), (b) $\Delta t=4.30$ (512×512 mesh), and (c) $\Delta t=2.15$ (1024×1024 mesh).

Table 1
Stability constraint of Δt for the proposed scheme.

Mesh size	$h=400/256$	$h=400/512$	$h=400/1024$
Time step	$\Delta t \le 20$ h	$\Delta t \le 15$ h	$\Delta t \le 12$ h

Table 2
Comparison of dimensionless steady-state tip velocities calculated by our proposed scheme ($V_{tip}=Vd_0/D$), calculated by phase-field simulations (V_{tip}^{KR}), and calculated by the Green function method (V_{tip}^{GF}).

Δ	ε_4	D	d_0/W_0	V_{tip}	V_{tip}^{KR}	V_{tip}^{GF}
0.65	0.05	1	0.554	0.0470	0.0465	0.0469
0.55	0.05	2	0.277	0.0171	0.0168	0.0170
0.55	0.05	3	0.185	0.0174	0.0175	0.0170
0.55	0.05	4	0.139	0.0172	0.0174	0.0170
0.50	0.05	3	0.185	0.01030	0.01005	0.00985
0.45	0.05	3	0.185	0.00599	0.00557	0.00545
0.45	0.05	4	0.139	0.00598	0.00540	0.00545

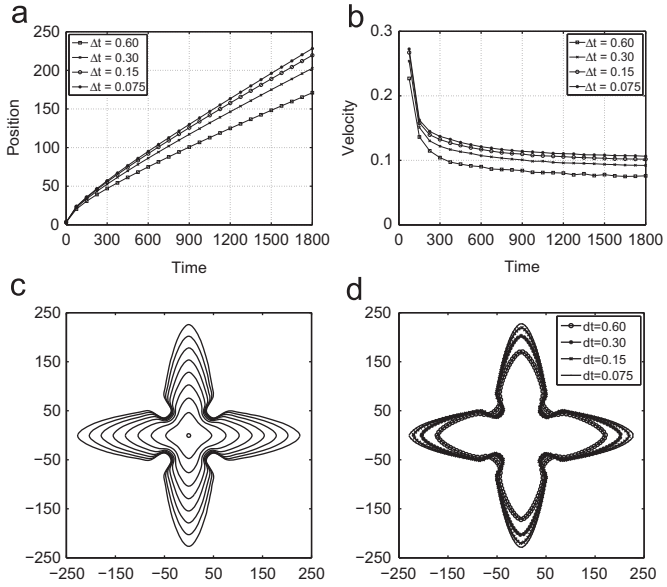

Fig. 3. (a) and (b) show the position and velocity of the tip versus time, respectively, for different time steps. (c) Evolutions of the interface with time step $\Delta t=0.15$. (d) The interfaces at time $T=1800$ for different time steps.

show sequences of interface for different mesh sizes. The position and velocity of the tip versus time are shown in Fig. 5(e) and (f), respectively. From the results shown in Fig. 5 we can observe that the spatial step size $h=0.3906$ is enough to simulate accurately and robustly the evolution of crystal growth.

Now we investigate the effects of radius of the initial solid seed and undercooling. For each test a 1024×1024 mesh is used on the domain $\Omega=(-400,400)^2$ and we choose $\Delta=-0.55$, $\Delta t=0.15$ and $T=1500$. The top row of Fig. 6 shows sequences of interfaces with different radii $R_0=15d_0$, $50d_0$, and $100d_0$ (from left to right). We can see that for an increase in the initial radius the dendrite grows faster. Sequences of interfaces with different undercooling sizes $\Delta=-0.45$, -0.55, and -0.65 are presented in the bottom row of Fig. 6. In this test we take $R_0=14d_0$. We observe that the large initial undercooling causes the dendrite to grow faster.

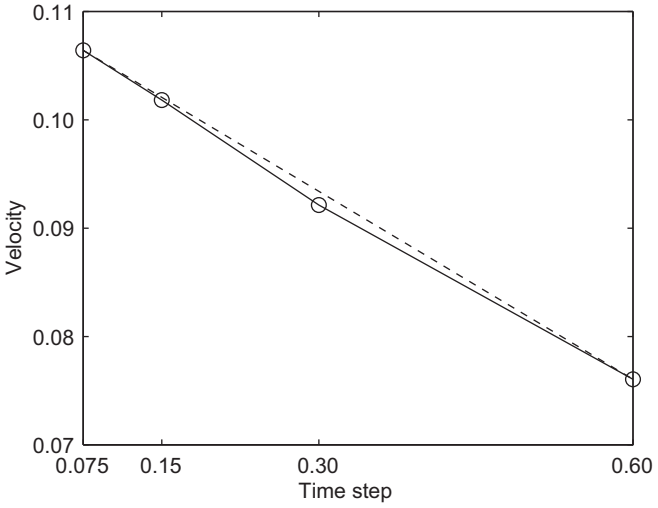

Fig. 4. The final velocity of the tip versus time step.

Table 3
Total CPU and average CPU ($\overline{\text{CPU}}$) times for different time steps.

Case	$\Delta t=0.6$	$\Delta t=0.3$	$\Delta t=0.15$	$\Delta t=0.075$
CPU time (h)	5.07	9.06	16.77	32.59
$\overline{\text{CPU}}$ time (s)	5.87	5.19	4.80	4.84

4.4. Three-dimensional crystal growth

In this section we consider a three-dimensional crystal growth. The initial conditions are

$$\phi(x,y,z,0)=\tanh\left(\frac{R_0-\sqrt{x^2+y^2+z^2}}{\sqrt{2}}\right),$$

$$U(x,y,z,0)=\begin{cases}0 & \text{if } \phi>0\\ \Delta & \text{else}\end{cases}$$

on the domain $\Omega=(-100,100)^3$ with a mesh $256\times256\times256$. The simulation parameters are $R_0=14d_0$, $\Delta=-0.55$, $\Delta t=0.15$, and $T=270$. Fig. 7 shows three-dimensional structures at different times. Structures with different undercooling sizes $\Delta=-0.45$, -0.55, and -0.65 at time $T=200$ are presented in Fig. 8(a)–(c), respectively. As in the two-dimensional experiment, we also observe that the large initial undercooling causes the dendrite to grow faster in three-dimensional crystal growth.

4.5. Tail morphology

Brener [43] derived a theory of the tail shape of a 3D needle crystal with the assumption that the cross section of a 3D needle crystal should grow as the time dependent 2D growth shapes away from the tip. In [27], Karma and Rappel compared the steady-state growth velocities from simulation and theory derived by Brener.

In this section we compare the velocities calculated by our scheme and those given in [27]. In 2D and 3D simulations, we choose $h=0.3906$, $R_0=14d_0$, $\Delta t=0.15$, and two different undercoolings $\Delta=-0.65$ and -0.70. In the 2D test a 1024×1024 mesh is used on the domain $\Omega=(-200,200)^2$ and the simulation time is

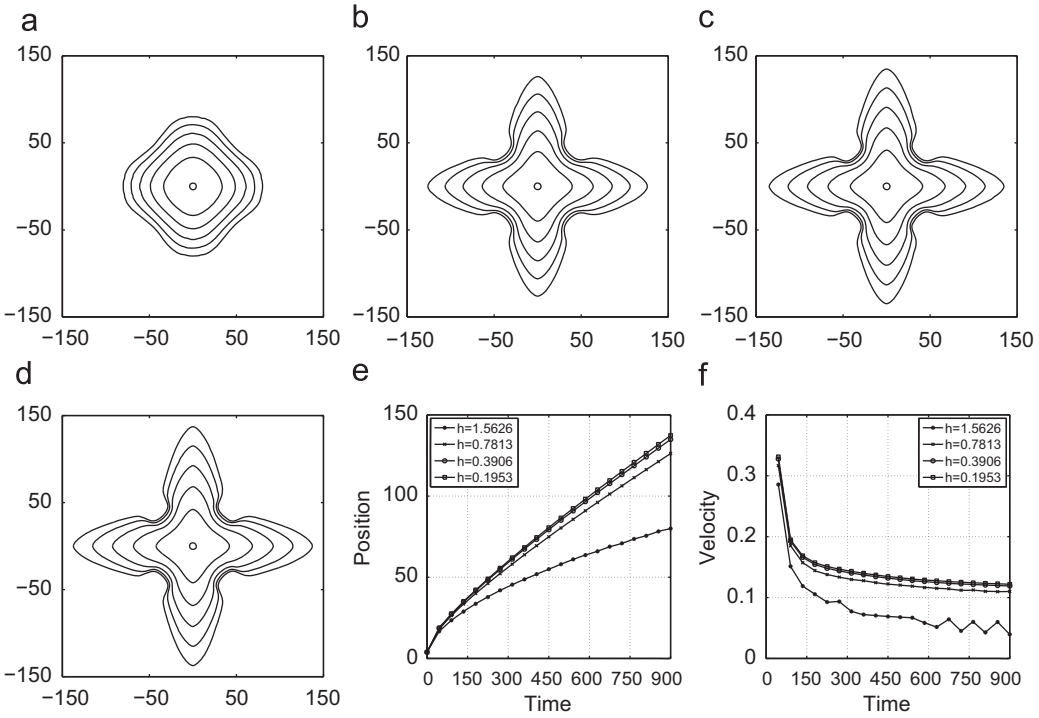

Fig. 5. Sequences of interfaces with different spatial step sizes: (a) $h=1.5626$, (b) $h=0.7813$, (c) $h=0.3906$, and (d) $h=0.1953$. (e) and (f) show the position and velocity of the tip versus time, respectively.

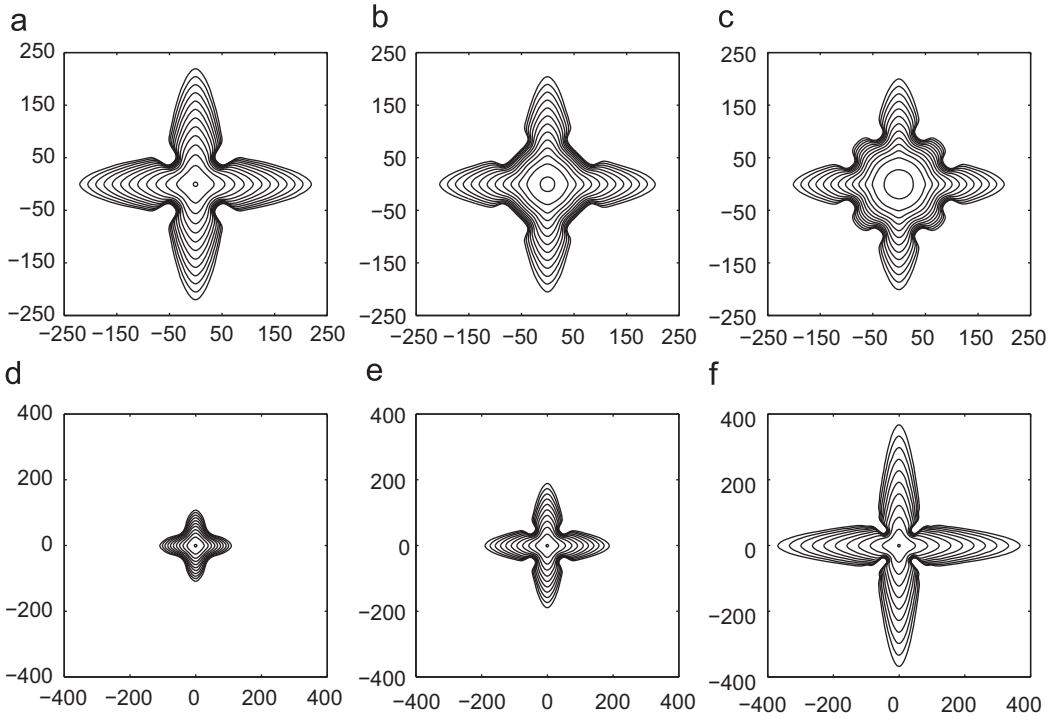

Fig. 6. Sequences of interfaces with different initial parameters. Top: evolutions of the dendrite with $R_0 = 15d_0$, $50d_0$, and $100d_0$. Bottom: evolutions of the dendrite with $\Delta = -0.45$, -0.55, and -0.65.

$T=750$. In the 3D test a $256\times256\times256$ mesh is used on the domain $\Omega=(-50,50)^3$ and the simulation time is $T=90$. Results of steady-state growth velocities obtained from 2D and 3D simulations are given in Table 4. Our results show good agreement with those of Karma and Rappel [27].

5. Conclusion

In this paper we proposed a fast, robust, and accurate operator splitting method for phase-field simulations of dendritic growth in both two- and three-dimensional space. The

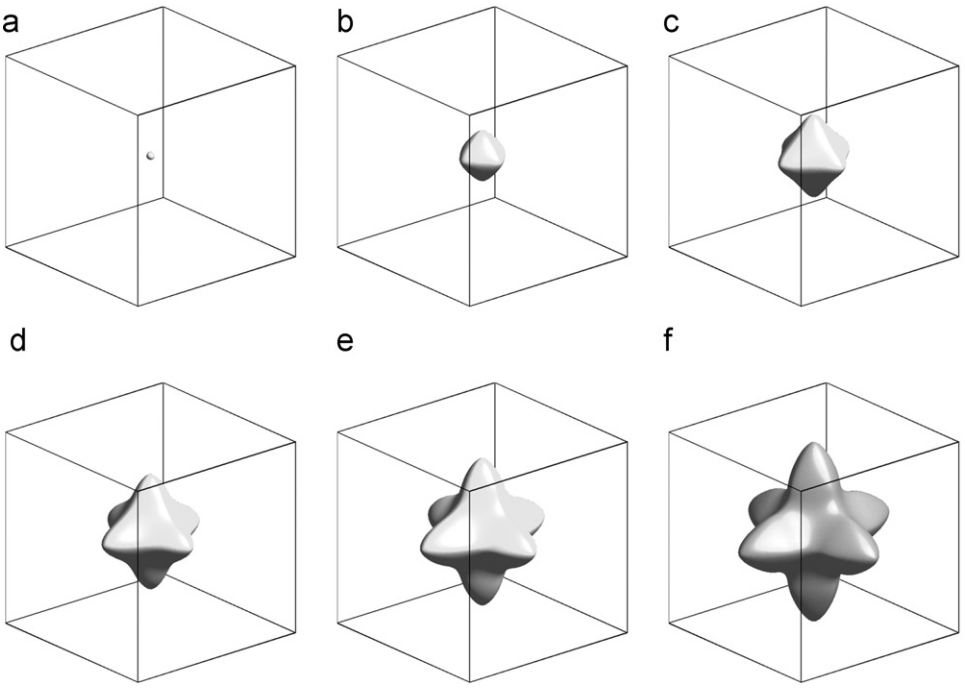

Fig. 7. Three-dimensional structures with $R_0 = 14d_0$ and $\Delta = -0.55$ at different times. (a) $t=0$, (b) $t=54$, (c) $t=108$, (d) $t=162$, (e) $t=216$, and (f) $t=270$.

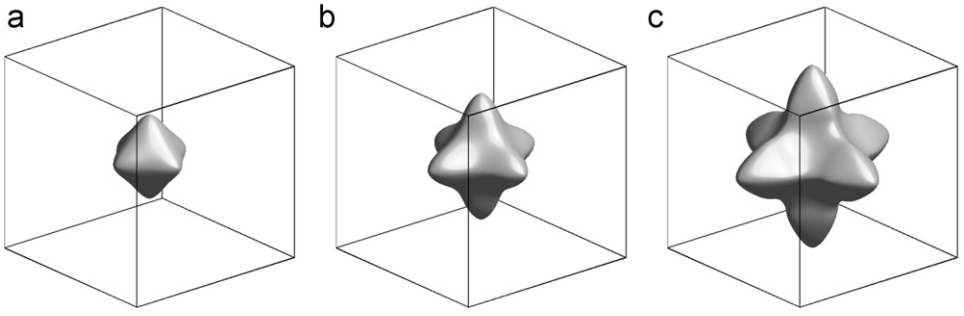

Fig. 8. Structures with different undercooling sizes (a) $\Delta = -0.45$, (b) $\Delta = -0.55$, and (c) $\Delta = -0.65$ at time $T = 200$.

Table 4
Results of steady-state growth velocities.

Δ	ε_4	V_{2D}	V_{3D}	V_{2D}/V_{3D}	V_{2D}^{KR}/V_{3D}^{KR}	Slope
−0.70	0.0294	0.0353	0.0813	0.434	0.44	0.43
−0.65	0.0294	0.0243	0.0620	0.392	0.39	0.40

proposed method is based on operator splitting techniques. We split the governing phase-field equation into three parts. The first equation is calculated explicitly, the second is a heat equation with a source term and is solved by a fast solver such as a multigrid method, and the third is evaluated using a closed form solution. We also presented a set of representative numerical experiments for crystal simulation to demonstrate the accuracy and efficiency of the proposed method. Our simulation results were also consistent with previous numerical experiments.

Acknowledgments

This work was supported by the National Research Foundation of Korea Grant funded by the Korean Government (MEST) (NRF-2010-0003989). The authors thank anonymous referee for very useful comments on this paper.

References

[1] S. Li, J.S. Lowengrub, P.H. Leo, Nonlinear morphological control of growing crystals, Phys. D 208 (2005) 209–219.
[2] D.I. Meiron, Boundary integral formulation of the two-dimensional symmetric model of dendritic growth, Phys. D 23 (1986) 329–339.
[3] J.A. Sethian, J. Strain, Crystal growth and dendlritic solidification, J. Comput. Phys. 98 (1992) 231–253.
[4] J. Strain, A boundary integral approach to unstable solidification, J. Comput. Phys. 85 (1989) 342–389.
[5] D. Li, R. Li, P. Zhang, A cellular automaton technique for modelling of a binary dendritic growth with convection, Appl. Math. Modelling 31 (2007) 971–982.
[6] H. Yin, S.D. Felicelli, A cellular automaton model for dendrite growth in magnesium alloy AZ91, Modelling Simul. Mater. Sci. Eng. 17 (2009) 075011.
[7] M.F. Zhu, C.P. Hong, A modified cellular automaton model for the simulation of dendritic growth in solidification of alloys, ISIJ Int. 41 (2001) 436–445.
[8] M.F. Zhu, S.Y. Lee, C.P. Hong, Modified cellular automaton model for the prediction of dendritic growth with melt convection, Phys. Rev. E 69 (2004) 061610.
[9] N. Al-Rawahi, G. Tryggvason, Numerical simulation of dendritic solidification with convection: two-dimensional geometry, J. Comput. Phys. 180 (2002) 471–496.
[10] T. Ihle, Competition between kinetic and surface tension anisotropy in dendritic growth, Eur. Phys. J. B 16 (2000) 337–344.

[11] D. Juric, G. Tryggvason, A front-tracking method for dendritic solidification, J. Comput. Phys. 123 (1996) 127–148.
[12] G. Tryggvason, B. Bunner, A. Esmaeeli, D. Juric, N. Al-Rawahi, W. Tauber, J. Han, S. Nas, Y.-J. Jan, A front-tracking method for the computations of multiphase flow, J. Comput. Phys. 169 (2001) 708–759.
[13] P. Zhao, J.C. Heinrich, D.R. Poirier, Fixed mesh front-tracking methodology for finite element simulations, Int. J. Numer. Meth. Eng. 61 (2004) 928–948.
[14] S. Chen, B. Merriman, S. Osher, P. Smereka, A simple level set method for solving Stefan problem, J. Comput. Phys. 135 (1997) 8–29.
[15] F. Gibou, R. Fedkiw, R. Caflisch, S. Osher, A level set approach for the numerical simulation of dendritic growth, J. Sci. Comput. 19 (2002) 183–199.
[16] Y.-T. Kim, N. Goldenfeld, J. Dantzig, Computation of dendritic microstructures using a level set method, Phys. Rev. E 62 (2000) 2471–2474.
[17] K. Wang, A. Chang, L.V. Kale, J.A. Dantzig, Parallelization of a level set method for simulating dendritic growth, J. Parallel Distrib. Comput. 66 (2006) 1379–1386.
[18] M. Plapp, A. Karma, Multiscale finite-difference-diffusion-Monte-Carlo method for simulating dendritic solidification, J. Comput. Phys. 165 (2000) 592–619.
[19] T.P. Schulze, Simulation of dendritic growth into an undercooled melt using kinetic Monte Carlo techniques, Phys. Rev. E 78 (2008) 020601(R).
[20] G. Caginalp, Stefan and Hele-Shaw type models as asymptotic limits of the phase-field equations, Phys. Rev. A 39 (1989) 5887–5896.
[21] C.C. Chen, C.W. Lan, Efficient adaptive three-dimensional phase-field simulation of dendritic crystal growth from various supercoolings using rescaling, J. Cryst. Growth 311 (2009) 702–706.
[22] C.C. Chen, Y.L. Tsai, C.W. Lan, Adaptive phase field simulation of dendritic crystal growth in a forced flow: 2D vs. 3D morphologies, Int. J. Heat Mass Transfer 52 (2009) 1158–1166.
[23] J.-M. Debierre, A. Karma, F. Celestini, R. Guérin, Phase-field approach for faceted solidification, Phys. Rev. E 68 (2003) 041604.
[24] J.-H. Jeong, N. Goldenfeld, J.A. Dantzig, Phase field model for three-dimensional dendritic growth with fluid flow, Phys. Rev. E 64 (2001) 041602.
[25] A. Karma, Y.H. Lee, M. Plapp, Three-dimensional dendrite-tip morphology at low undercooling, Phys. Rev. E 61 (2000) 3996–4006.
[26] A. Karma, W.-J. Rappel, Phase-field method for computationally efficient modeling of solidification with arbitrary interface kinetics, Phys. Rev. E 53 (1996) R3017–R3020.
[27] A. Karma, W.-J. Rappel, Quantitative phase-field modeling of dendritic growth in two and three dimensions, Phys. Rev. E 57 (1998) 4323–4349.
[28] R. Kobayashi, Modeling and numerical simulations of dendritic crystal growth, Phys. D 63 (1993) 410–423.
[29] N. Provatas, N. Goldenfeld, J. Dantzig, Efficient computation of dendritic microstructures using adaptive mesh refinement, Phys. Rev. Lett. 80 (1998) 3308–3311.
[30] N. Provatas, N. Goldenfeld, J. Dantzig, Adaptive mesh refinement computation of solidification microstructures using dynamic data structures, J. Comput. Phys. 148 (1999) 265–290.
[31] J.C. Ramirez, C. Beckermann, A. Karma, H.-J. Diepers, Phase-field modeling of binary alloy solidification with coupled heat and solute diffusion, Phys. Rev. E 69 (2004) 051607.
[32] J. Rosam, P.K. Jimack, A. Mullis, A fully implicit, fully adaptive time and space discretisation method for phase-field simulation of binary alloy solidification, J. Comput. Phys. 225 (2007) 1271–1287.
[33] C.J. Shih, M.H. Lee, C.W. Lan, A simple approach toward quantitative phase field simulation for dilute-alloy solidification, J. Cryst. Growth 282 (2005) 515–524.
[34] X. Tong, C. Beckermann, A. Karma, Q. Li, Phase-field simulations of dendritic crystal growth in a forced flow, Phys. Rev. E 63 (2001) 061601.
[35] S.-L. Wang, R.F. Sekerka, Algorithms for phase field computation of the dendritic operating state at large supercoolings, J. Comput. Phys. 127 (1996) 110–117.
[36] J.A. Warren, W.J. Boettinger, Prediction of dendritic growth and microsegregation patterns in a binary alloy using the phase-field method, Acta Metall. Mater. 43 (1995) 689–703.
[37] Y. Xu, J.M. McDonough, K.A. Tagavi, A numerical procedure for solving 2D phase-field model problems, J. Comput. Phys. 218 (2006) 770–793.
[38] A. Jacot, M. Rappaz, A pseudo-front tracking technique for the modelling of solidification microstructures in multi-component alloys, Acta Mater. 50 (2002) 1909–1926.
[39] J.S. Langer, Directions in Condensed Matter, World Scientific, Singapore, 1986, pp. 164–186.
[40] A.M. Stuart, A.R. Humphries, Dynamical Systems and Numerical Analysis, Cambridge University Press, New York, 1998.
[41] W.L. Briggs, A Multigrid Tutorial, SIAM, Philadelphia, 1987.
[42] U. Trottenberg, C. Oosterlee, A. Schüller, Multigrid, Academic Press, USA, 2001.
[43] E. Brener, Needle-crystal solution in three-dimensional dendritic growth, Phys. Rev. Lett. 71 (1993) 3653–3656.